crystals

MDPI

Article

The Effect of AlN Content on the Properties of Al_2O_3-AlN Composite Ceramics Fabricated by Digital Light Processing

Shaocong He †, Yehua Li †, Xiao Zong * and Shanghua Wu

School of Electromechanical Engineering, Guangdong University of Technology, Guangzhou 510006, China
* Correspondence: zongxiao@gdut.edu.cn
† These authors contributed equally to this work.

Abstract: In this work, Al_2O_3-AlN composite ceramics with high bending strength and thermal conductivity were fabricated by Digital Light Processing (DLP). The influence of AlN content on the rheological and cure behavior of Al_2O_3-AlN suspensions, as well as the microstructure, thermal conductivity, and bending strength of Al_2O_3-AlN ceramics, were systematically investigated. The result shows that the viscosity and cure ability of the suspensions were decreased with the increase of AlN content, which are beneficial to the spreading and printing accuracy of the suspensions. Besides, the bending strength of ceramics can be improved due to the residual stress by the introduction of AlN. Approaches were employed to minimize the formation of AlON in Al_2O_3-AlN ceramics by optimizing the amount of AlN and the sintering temperature. The thermal conductivity and bending strength of Al_2O_3-AlN ceramics were 31.72 ± 0.45 W/(m·K) and 572.73 ± 59.40 MPa, respectively, which are much higher than those of Al_2O_3 ceramics fabricated under the same condition. Finally, complex-shaped Al_2O_3-AlN ceramics components have been successfully fabricated by DLP, which may provide an opportunity to broaden the application of Al_2O_3-AlN composite ceramics in heat dissipation components.

Keywords: Al_2O_3-AlN composite ceramics; Digital Light Processing; mechanical properties; thermal conductivity

check for updates

Citation: He, S.; Li, Y.; Zong, X.; Wu, S. The Effect of AlN Content on the Properties of Al_2O_3-AlN Composite Ceramics Fabricated by Digital Light Processing. *Crystals* **2023**, *13*, 107. https://doi.org/10.3390/cryst13010107

Academic Editor: Francisco M. Morales

Received: 22 December 2022
Revised: 31 December 2022
Accepted: 2 January 2023
Published: 6 January 2023

Copyright: © 2023 by the authors. Licensee MDPI, Basel, Switzerland. This article is an open access article distributed under the terms and conditions of the Creative Commons Attribution (CC BY) license (https://creativecommons.org/licenses/by/4.0/).

1. Introduction

Alumina ceramics (Al_2O_3) is widely used in support substrates in integrated circuits and heat-dissipating LED substrates, and electronic substrates for high-temperature semiconductor packages, because of high bending strength, hardness, low electrical conductivity, and low-priced cost of production [1,2]. However, the application of Al_2O_3 ceramics in integrated circuits and electronic components is greatly restricted for the reason that the thermal conductivity of Al_2O_3 ceramics is less than 30 W/(m·K). Compared with Al_2O_3 ceramics, the thermal conductivity of AlN ceramics can reach 319 W/(m·K) in theory. Besides, AlN ceramics more match the thermal expansion coefficient with silicon [3,4] (4.6×10^{-6} K^{-1} at 20–500 °C). However, low bending strength, low oxidation resistance, and high production cost are problems for AlN ceramics [5]. Therefore, Al_2O_3-AlN ceramic composites are regarded as an option to realize their complementary advantages, where Al_2O_3 promotes the mechanical property of AlN ceramics and AlN provides high thermal conductivity for Al_2O_3 ceramics, decreasing the coefficient of thermal expansion [6,7].

However, it is difficult to process Al_2O_3-AlN composite ceramics with the desired shape due to the high hardness and brittleness. The complex shape of ceramic parts is conducive to improving the performance of heat dissipation, in which the ratio of ceramic parts surface, a cooling channel within the structure, and the volume of components have a great effect [8,9]. Nowadays, conventional methods applied to fabricate the Al_2O_3-AlN ceramics require molds and post-machining, which are expensive and time-consuming. Besides, the traditional forming methods hardly meet the requirements for the preparation of

ceramics with complex shapes. Additive manufacturing can directly prepare components with complicated shapes and high precision. Stereolithography (SL), especially Digital Light Processing (DLP), is regarded as a promising 3D printing technique and has been developing rapidly due to its high precision and the ability to fabricate complex-shaped ceramic components with great surface quality [10,11]. In recent years, the DLP technique has been widely applied to fabricate ceramic components with complex shapes and optimized structures, and applied in different fields in terms of heat exchange [8], static mixers in the chemical industry, radiator parts in large-scale integrated circuits [4] and ceramic core in the aircraft engines [12]. Consequently, DLP technology can be applied to prepare ceramic components with complicated shapes, which is beneficial to give scope to the excellent properties of Al_2O_3-AlN composite ceramics.

The critical factor to DLP is the rheological properties and cure behaviors of ceramic slurry [13,14]. Due to the low intrinsic surface charge of nitride ceramics, the suspension of nitride ceramics has weaker shear thinning and higher viscosity, which affects the preparation of high solid loading slurry [15,16]. Besides, compared with Al_2O_3, AlN has higher absorbance of light and refractive index [17]. The large refractive index difference between ceramics and resin will result in the decline of cure depth [13,18]. In this regard, it is worth studying the influence of AlN content on the viscosity, stability, and cure behaviors of the slurries. Moreover, the properties of Al_2O_3-AlN ceramics will be affected by the content of AlN. Previous research shows that the AlON phase with a thermal conductivity of about 10 W/(m·K) is easily formed in the Al_2O_3-AlN system. The formation of AlON will result in the rapid decline of thermal conductivity in the Al_2O_3-AlN system [19]. Besides, the reaction between Al_2O_3 and AlN may introduce defects in sintered body, thus affecting mechanical properties. To date, many studies pay attention to the phase formation in the Al_2O_3-AlN system. Kim et al. [20] found that the increase of AlN addition and temperature further enhanced the reaction of Al_2O_3 and AlN, which led to a large number of AlON. However, the formation of AlON was delayed until 1700 °C in a ternary Al_2O_3-AlN-Y_2O_3 system [19]. Besides, Hu et al. [21] prepared Al_2O_3-AlN composites by pressureless sintering. With optimized AlN content(10 wt%) and sintering temperature (1600 °C), Al_2O_3-AlN composites achieved the best properties in terms of the bending strength of 295.7 MPa and thermal conductivity of 38.8 W/(m·K). It can be concluded from the previous research work that AlN content and sintering temperature are important factors affecting the properties of Al_2O_3-AlN ceramics. Furthermore, the relative density of ceramic green bodies obtained by DLP is always lower than that by other forming methods, and thus it is necessary to optimize AlN content and sintering temperature to fabricate Al_2O_3-AlN ceramics with excellent comprehensive properties by DLP [22–25].

This study aims at investigating the effects of the addition of AlN on the rheological properties, stability, and curing behaviors of ceramic slurries. The effects of AlN content and sintering temperature on relative density, microstructure, thermal conductivity, and bending strength of Al_2O_3-AlN composite ceramics fabricated by DLP are also discussed. It focuses on the optimization of AlN content and sintering temperature for the fabrication of the Al_2O_3-AlN composites ceramic part with high properties and complex shape.

2. Experimental Procedures

2.1. Material

Commercial α-Al_2O_3 powder (D_{50} = 200 nm, TM-DAR, Taimei Chemicals Co., Ltd., Tokyo, Japan) and AlN powder (D_{50} = 1.30 μm, Grade JC, Toyo Aluminium, Toyo, Japan) were used in this study. Yttrium oxide (Y_2O_3) powder was used as the sintering aid (D_{50} = 0.5 μm, Macklin Biochemical Co., Ltd., Shanghai, China). The photosensitive resins used in this study contained 1,6-hexanediol diacrylate (HDDA, Shanghai Guangyi Chemical Co., Ltd., Shanghai, China), ethoxylated pentaerythritol tetraacrylate (PPTTA, Shanghai Guangyi Chemical Co., Ltd., Shanghai, China), and dioctyl phthalate (DOP, 99.0% purity, Aladdin Bio-Chem Technology Co., Ltd., Shanghai, China). The photoinitiator used was 2,4,6-trimethylbenzoyl (Royal DSM). Oleic Acid (Aladdin Bio-Chem Technology Co., Ltd.,

Shanghai, China) was used as a powder modifier, and KOS110 (Guangzhou Kang'oushuang Trade Co., Ltd., Guangzhou, China) was used as a dispersant.

2.2. Sample Preparation

The composite powders were planetary ball milled in absolute ethanol for 8 h at the speed of 350 r/min according to different mass ratios of AlN powder, where the content of AlN is 5, 10, 15, 20 wt%, the content of Y_2O_3 is 5 wt%, and Oleic Acid is kept for 1 wt%. Then the composite powders were dried in an oven at 50 °C and passed through the 100-mesh sieve. The suspensions were fabricated by mixing ceramics powders, resins, and a photoinitiator with ball milling at a speed of 350 r/min for 2 h. The suspensions were cured to a specific shape with the DLP machine (tc-1, Zhejiang Xunshi Technology Co., Ltd., Shaoxing, China). The bland sample was 5 wt%Y_2O_3-95 wt%Al_2O_3. The debinding process was as follows: a two-step debinding process was used. The debinding process contained vacuum debinding and air debinding. The heating rate was 1 °C/min, and heat preservation for 1 h every 100 °C rose up to 450 °C. After debinding, green bodies were heated to 1600 °C, 1650 °C, and 1700 °C, respectively, at a heating rate of 5 °C/min and kept at the highest temperature respectively for 2 h.

2.3. Characterization

The viscosity of the ceramic suspensions was measured by a rotational rheometer ((MCR301, Physica, Vienna, Austria). The absorbance of ceramic powders was measured by an ultraviolet-visible spectrophotometer (UV-3600 Plus, Shimadzu, Tokyo, Japan). The excess cure width and cure depth are measured by a stereomicroscope (CDM-806H2, Tuming, Hong Kong, China) and a spiral micrometer. X-ray diffraction (XRD, D8 Advance, Bruker Corporation, Ettlingen, Germany) was used to analyze the phase composition of the ceramic sample. The microstructures of ceramic samples were observed by scanning electron microscopy (SEM; SU8220, Hitachi, Tokyo, Japan) with deionized water as a medium, using Archimedes' principle to determine the density. The bending strength was measured by the span three points blending method, with the dimension of 1.5 × 2 × 25 mm. Five samples were tested to take the average value. The laser thermal conductivity instrument (LFA447, NETZSCH, Selb, Germany) was applied to measure the thermal diffusivity (α). The dimension of the specimens was 10 × 10 × 2 mm and the test temperature was room temperature. The thermal conductivity (κ) can be calculated as follows [26]:

$$\kappa = \rho \cdot C_p \cdot \alpha \tag{1}$$

where ρ is the density, α is the thermal diffusivity at room-temperature, C_p is the heat capacity. The Neumann–Kopp rule was applied to calculate the heat capacity of sintered capacity of sintered Al_2O_3-AlN composites ceramic [27]:

$$C_p(AB) = w_A \cdot C_p(A) + w_B \cdot C_p(B) \tag{2}$$

where $C_p(AB)$ is the heat capacity of samples, w_A and w_B are the mass fractions and $C_p(A)$, $C_p(B)$ is the heat capacity of Al_2O_3 and AlN, respectively. The change in heat capacity caused by sintering additives is low, which is neglected [28].

3. Results and Discussion

3.1. Rheology and Stability of the Ceramic Suspensions

The rheological behavior of the suspensions with different content of AlN presented by viscosity curves is shown in Figure 1. Shear thinning behavior was observed in all suspensions. It shows that compared with pure Al_2O_3 suspension, the viscosity of the suspension containing AlN powders is significantly lower. As the content of AlN increased, the viscosity of the ceramic suspensions decreased. The average particle size of Al_2O_3 powders is 200 nm, while that of AlN powders is much larger (1.30 μm), which can significantly reduce the friction between the particle [29].

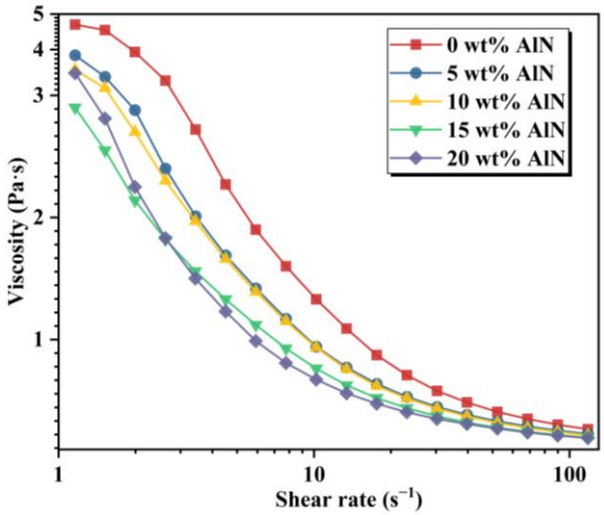


Figure 1. Viscosity versus shear rate curves of suspensions with different content of AlN powders.

The stability of suspensions, which is always affected by the agglomeration and sedimentation of the ceramic powders, is an important factor to be considered. The diagram of the sedimentation test is exhibited in Figure 2a. The solid loading of suspensions was maintained at 10 vol%, and the amount of AlN varied from 0 to 20 wt%. The sedimentation distance of different AlN content and time are shown in Figure 2b–d. The results show that the suspensions containing AlN powders had higher sedimentation height compared with the pure Al_2O_3 suspension in Figure 2b. This phenomenon indicates that the addition of AlN with large particle size accelerates the rate of suspension sedimentation. Furthermore, with the increase of AlN content, the sedimentation of the slurry becomes more serious, and the stability of the slurry becomes worse. This can be explained by Equation (3) [14]:

$$u_0 = \frac{g\left(\rho_s - \rho_f\right)d^2}{18\eta_f} \tag{3}$$

where ρ_s is the density of ceramics, ρ_f is the density of resin, d is mean diameter of ceramic powders, η_f is the viscosity of the resin, u_0 is the falling rate of particles. Therefore, as the mean diameter of Al_2O_3-AlN composite powders increases with the addition of AlN, the falling rate of particles has been accelerated.

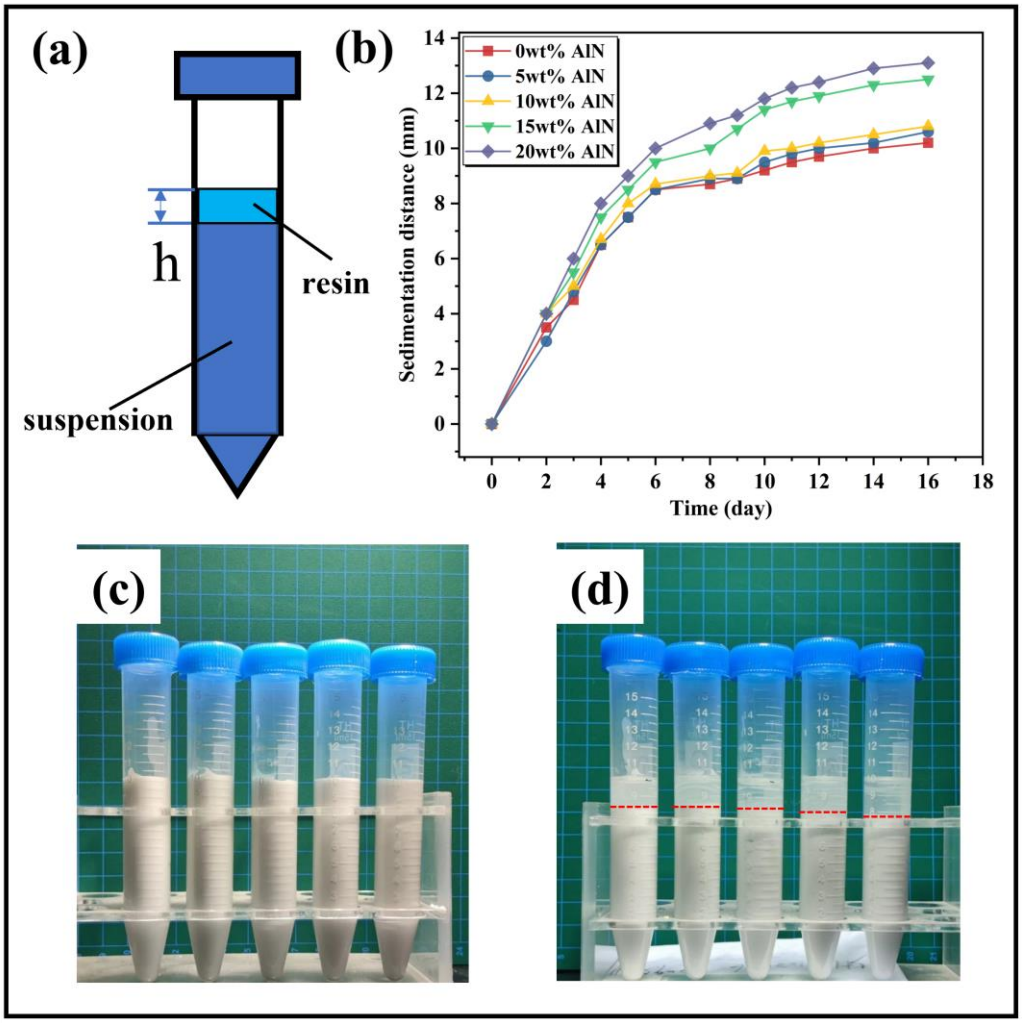


Figure 2. (**a**) Diagram of sedimentation distance; (**b**) Sedimentation height of the suspensions with different content of AlN after different times; (**c**) Photograph of sedimentation distance after 0 days; (**d**) Photograph of sedimentation distance after 14 days.

3.2. Curing Behavior of the Ceramic Suspensions

To demonstrate the influence of AlN powders on the curing behavior of suspensions, cure depth, and excess cure width of the suspensions with 50 vol% solid loading were measured and presented in Figure 3. Cure depth (C_d) can be calculated below [30]:

$$C_d = S_d \ln\left(\frac{E}{E_c}\right) \tag{4}$$

where C_d is the cure depth, S_d is the depth sensitivity, E is the incident energy, E_c is the critical energy. The excess cure width (W_{ex}) follows the Beer–Lambert law [30]:

$$W_{ex} = S_w \ln\left(\frac{E}{E_w}\right) \tag{5}$$

where S_w is the width sensitivity, E_w is the critical energy. Besides, the ideal suspension has enough cure depth but no excess cure width. This can be characterized by broadening width (D_b) calculated by Equation (5) [13,30]:

$$D_b = S_d \ln\left(\frac{E_c}{E_w}\right) \tag{6}$$

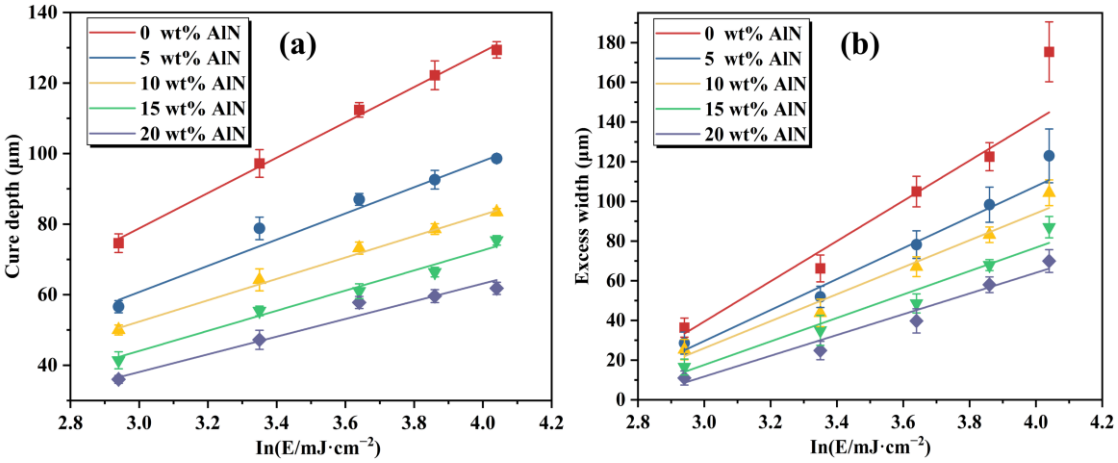


Figure 3. (**a**) The relation of the cure depth and the exposure energy density; (**b**) The relation of the excess cure width and exposure energy density.

The cure depth and excess width were increased with the enhancement of energy in Figure 3. Besides, cure depth and excess width decreased with the increase of AlN content, which indicates that AlN as an additive has adverse effects on the cure capability of the ceramic suspension. However, lower excess width can be beneficial to the high printing precision during the process of DLP [30]. To characterize the effect of AlN content on the cure capability, S_d, $S_{w,}$ and D_b were calculated according to Equations (4)–(6). The results are presented in Table 1. It shows that S_d, $S_{w,}$ and D_b of Al_2O_3-AlN suspensions are reducing with the increase of AlN content. S_d, $S_{w,}$ and D_b decrease from 50.06 to 25.07 μm, 101.39 to 52.31 μm, and 42.23 to 19.36 μm, respectively, which can bring better control of the printing precision. As AlN powders absorb more ultraviolet light, it results in the decline of cure ability. The absorptance of the ceramic powders, with AlN powders content varying from 0 to 20 wt%, was measured in 405 nm wavelength to prove the conclusion. As presented in Figure 4, the absorbance of the Al_2O_3-AlN increased four times at least compared with the Al_2O_3 powders, and it also raised with the increase of AlN content, which confirms the above inference.

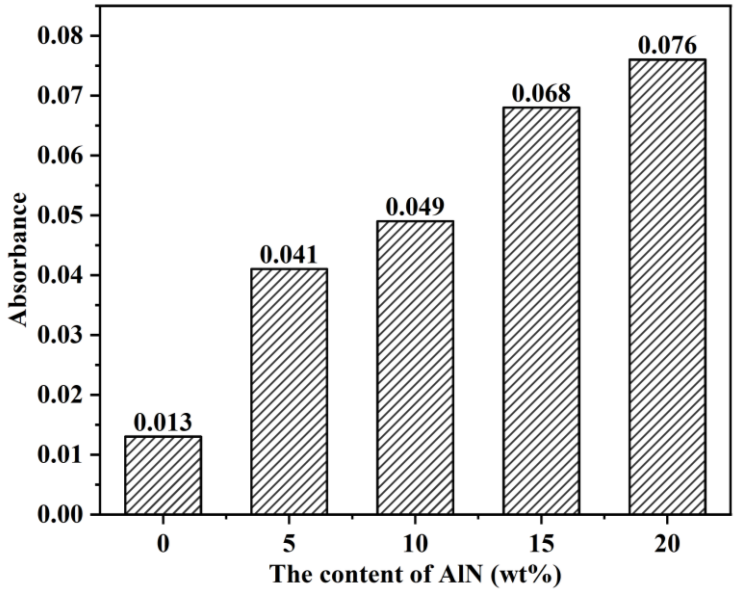


Figure 4. The absorbance of the Al_2O_3-AlN powders with 0–20 wt% AlN at 405 nm wavelength.

The addition of AlN is conducive to improving rheological behavior and printing accuracy, while it has the opposite influence on curing performance and stability. When the content of AlN is 15 and 20 wt%, the viscosity of ceramic suspensions can meet the requirement of DLP, but the cure depth and stability of suspensions decrease when the AlN content increases. Thus, 15 wt% is the optimum content of AlN for preparing suspension by comprehensively considering viscosity, stability, cure depth, and printing accuracy.

Table 1. Depth sensitivity (S_d), width sensitivity (S_w), and broadening depth (D_b) of the suspensions with different AlN content.

The Content of AlN (wt%)	S_d (μm)	S_w (μm)	D_b (μm)
0	50.06	101.39	42.23
5	37.14	78.00	29.58
10	30.28	67.95	22.50
15	28.53	56.62	20.90
20	25.07	52.31	19.36

3.3. Relative Density and Microstructure of the Sintered Al_2O_3-AlN Ceramics

After debinding, the ceramic samples were sintered at 1600 °C, 1650 °C, and 1700 °C for 2 h with nitrogen gas, respectively. The phase compositions of the Al_2O_3-AlN ceramic samples with different AlN content and sintering temperature are shown in Figure 5. The sintered samples at 1650 °C are composed of Al_2O_3, AlN, and YAG ($Y_3Al_5O_{12}$) phases, and the sintered samples at 1700 °C consist of Al_2O_3, AlN, YAG, and AlON phases. These phenomena are consistent with other relevant research results [19,20]. The AlON formed by the reaction between Al_2O_3 and AlN will have a negative impact on the properties of ceramics. As can be seen in Table 2, the relative densities of specimens with different AlN content were all below 80% at 1600 °C because of insufficient sintering driving force, which resulted in the non-densified ceramics. The linear shrinkage of the sintering bodies at 1650 °C with different AlN content is shown in Figure 6. There is no significant difference in the contraction of samples with different content of AlN in the x, y, and z directions. The shrinkage of samples with the same AlN content in the z direction is larger than that of samples in the x and y directions. This may be attributed to the deposition of particles in the spreading layer caused by squeegee movement during the printing process, as well as the rearrangement and densification of particles caused by gravity along the z direction during the sintering process [31]. Relative densities of the samples were improved significantly when the sintering temperature was raised to 1650 °C. However, the relative densities decreased as the sintering temperature increased from 1650 °C to 1700 °C, which may be due to the formation of AlON. The reaction of Al_2O_3 and AlN at 1700 °C can be presented below [19]:

$$Al_2O_3 + AlN \rightarrow Al_3O_3N. \quad (7)$$

Table 2. The relative density of sintered samples at different temperatures.

The Content of AlN (wt%)	Relative Density (%)		
	1600 °C	1650 °C	1700 °C
0	79.13 ± 0.20	97.82 ± 0.15	97.03 ± 0.36
5	73.97 ± 0.41	99.24 ± 0.11	97.90 ± 0.21
10	71.84 ± 0.10	99.13 ± 0.07	97.71 ± 0.35
15	65.23 ± 0.19	98.83 ± 0.17	97.16 ± 0.15
20	64.05 ± 0.12	97.90 ± 0.22	96.99 ± 0.27

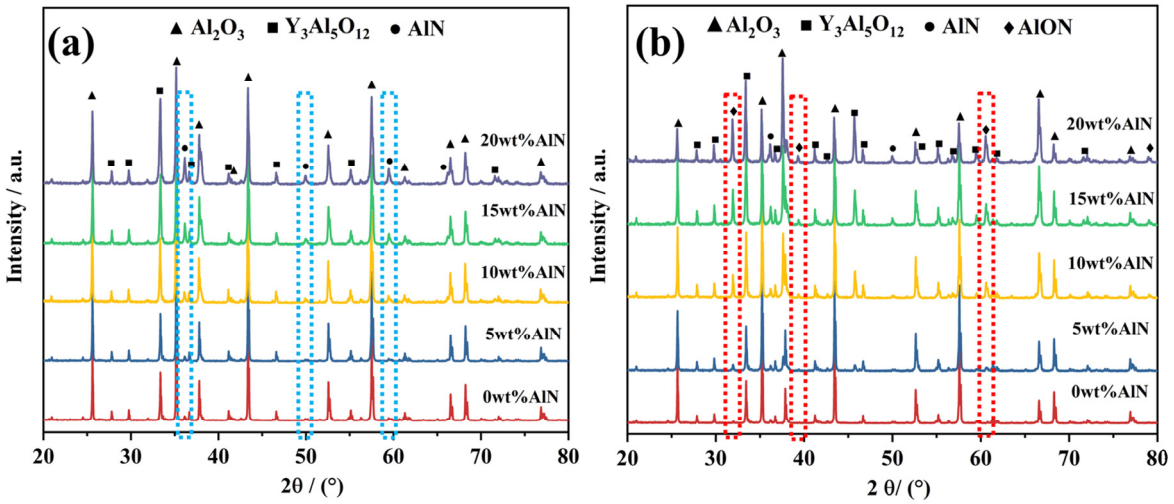


Figure 5. Normalized XRD patterns of Al_2O_3-AlN composites at different temperatures: (**a**) 1650 °C, (**b**) 1700 °C.

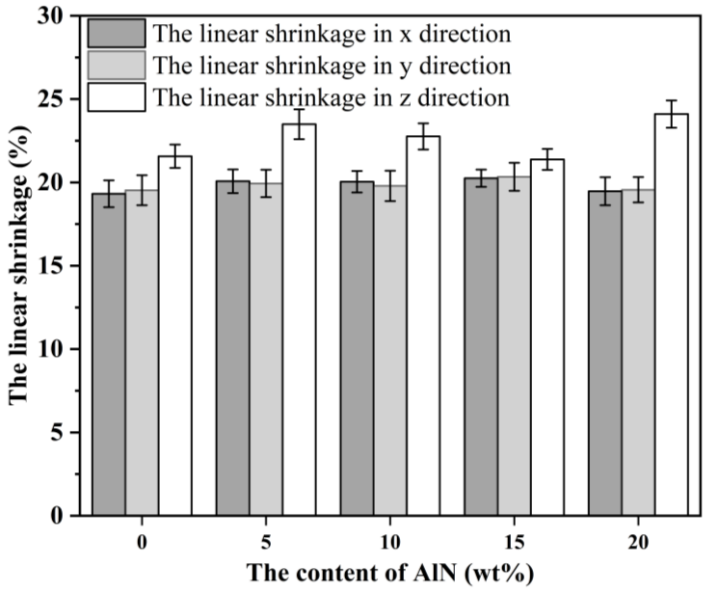


Figure 6. The linear shrinkage of sintering samples at 1650 °C with different AlN content.

Al_3O_3N, also called AlON, has a larger specific volume than the Al_2O_3 matrix [19]. The formation of AlON replaced the Al_2O_3 matrix, resulting in the displacement of the matrix, in which large voids are generated [20,32]. Thus, the porosity of samples sintered at 1700 °C increased.

Figure 7 shows the microstructures of the samples sintered at 1650 °C with different AlN content. The mean grain sizes of Al_2O_3-AlN composites at 1650 °C are indicated in Table 3, Al_2O_3 grains grew abnormally in Figure 7a, which results in intercrystallite and intragranular pore. Figure 7b–d and Table 3 show that the grains of ceramics are refined obviously with the addition of AlN due to the inhibition of Al_2O_3 grain growth by AlN. Besides, the relative density was promoted when AlN content varied from 5 to 15 wt%. However, when the content of AlN reached 20 wt%, the relative density decreased obviously. AlN has a high covalent bonding, and its self-diffusion coefficient is low, so the addition of a large amount of AlN will cause difficulty in the densification of ceramics [33].

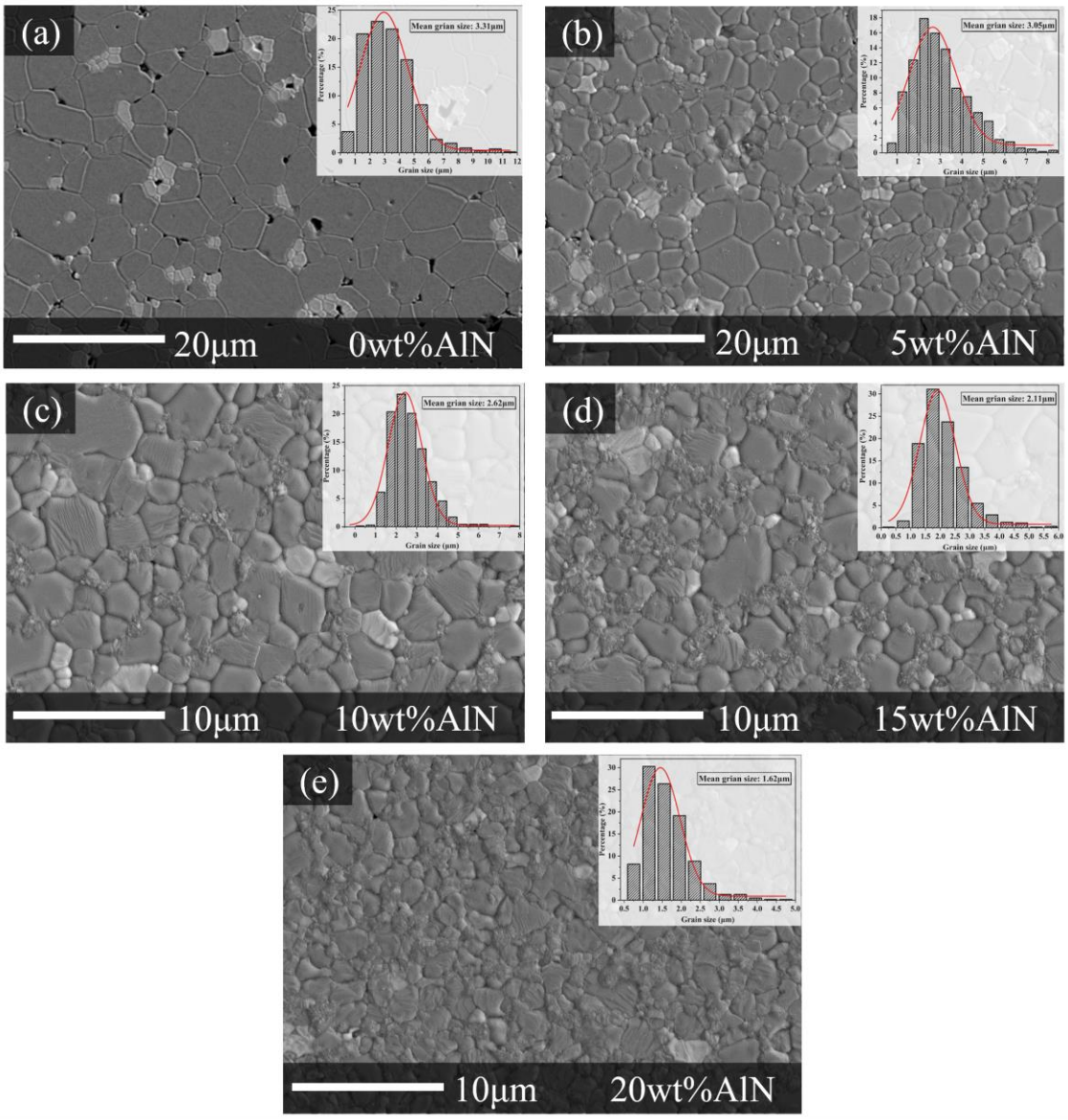


Figure 7. Microstructure and grain size distribution at 1650 °C 2 h: (**a**) 0 wt% AlN; (**b**) 5 wt% AlN; (**c**) 10 wt% AlN; (**d**) 15 wt% AlN; (**e**) 20 wt% AlN.

Table 3. Bending strength and mean grain size of Al_2O_3-AlN composites at 1650 °C for 2 h.

AlN Content (wt%)	0	5	10	15	20
Bending strength (MPa)	345.95 ± 43.98	500.35 ± 62.04	513.90 ± 52.27	572.73 ± 59.40	534.51 ± 60.11
Mean grain size (μm)	3.31	3.05	2.62	2.11	1.62

3.4. Thermal and Mechanical Properties of the Sintered Al_2O_3-AlN Ceramics

The effect of AlN content on the thermal conductivity of samples at different sintering temperature are displayed in Figure 8. When AlN content was increased from 0 to 15 wt% at 1650 °C, the thermal conductivity of Al_2O_3-AlN ceramics improved from 28.87 to 31.72 W/(m·K). As AlN has a higher thermal conductivity compared with Al_2O_3, it is conducive to improving thermal conductivity of Al_2O_3-AlN ceramics. When AlN content increased from 15 to 20 wt%, the improvement of thermal conductivity was slow, only

increasing from 31.72 to 32.36 W/(m·K). This phenomenon can be attributed to grain refinement and the decline of density, which enhanced phonon scattering and decreased the phonon mean free path [3]. Besides, the thermal conductivity of Al_2O_3-AlN composites at 1700 °C decreased as AlN content increased, which may be due to the formation of AlON. The XRD spectrum was normalized to compare the intensity of diffraction peaks of the AlON. The intensity of the AlON diffraction peak increased significantly when AlN content increased in Figure 5b. AlON has low thermal conductivity [19] (about 10 W/(m·K)) and increases porosity in sintered body, which results in the decline of thermal conductivity rapidly at 1700 °C.

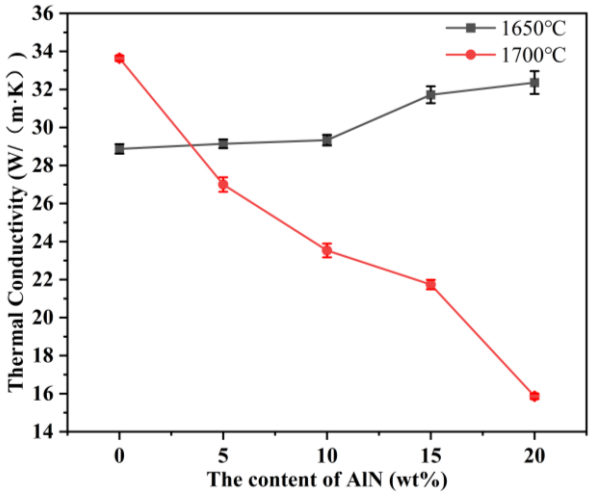


Figure 8. Thermal conductivity of Al_2O_3-AlN composites at 1650 °C and 1700 °C.

Considering the existence of AlON at 1700 °C seriously affects the density and thermal conductivity of the ceramic, 1650 °C was selected as the best sintering temperature. The bending strength of ceramics sintered at 1650 °C is shown in Table 3. Notably, the bending strength of the blank sample without the addition of AlN had the lowest value of 345.95 ± 43.98 MPa, which presents that the addition of AlN is able to promote bending strength significantly. This may be attributed to the residual stress caused by the mismatch of the thermal expansion coefficient between the Al_2O_3 matrix and AlN [21,34], which is an important factor for enhancing mechanical properties. The thermal expansion coefficient (TEC) of Al_2O_3 is 9.2–9.6 × 10^{-6} K^{-1} [1], almost twice as high as that of AlN (~4.8 × 10^{-6} K^{-1}) [3], which results in the Al_2O_3 under the compressive stress at the room temperature. As the compressive stress strengthens the grain boundary, microcracks are forced to diverge and deflect along the Al_2O_3/AlN interface, consuming more energy to propagate. Therefore, bending strength of Al_2O_3/AlN composites were enhanced. In addition, grain size is another important factor to influence bending strength. The fine grain size can decrease the size of the inherent flaw, improving bending strength for polycrystalline material [35,36]. As the content of AlN increased from 0 to 20 wt%, the grains of Al_2O_3-AlN ceramics were obviously refined, as shown in Table 3 and Figure 7. Under the combined effect of residual stress and grain refinement, the bending strength gradually enhanced with the increase of AlN content from 0 to 15 wt%. However, the bending strength of the ceramic with 20 wt% AlN decreased slightly, which was caused by the non-densified microstructure. The pores in Al_2O_3-AlN composites reduced the force area and caused stress concentration at which ceramic fracture was more likely to occur [37]. When the content of AlN was 15 wt%, bending strength reached the highest value of 572.73 ± 59.40 MPa, 65.56% higher than that of the blank sample.

Thus, Al_2O_3-AlN composites via DLP achieved the best results in terms of bending strength of 572.73 ± 59.40 MPa and thermal conductivity of 31.72 W/(m·K), when AlN content was 15 wt%, and sintering temperature was 1650 °C. The thermal conductivity and bending strength of Al_2O_3-AlN ceramics fabricated by different methods are listed in

Table 4. The thermal conductivity of Al_2O_3-AlN ceramics prepared by DLP is close to that of other preparation methods, but the bending strength is improved.

Table 4. Bending strength and thermal conductivity of Al_2O_3-AlN ceramics fabricated by different methods.

Specimen	Preparation Method	Bending Strength (MPa)	Thermal Conductivity (W/(m·K))
10 wt% AlN-Al_2O_3 [21]	cold isostatic pressing	295.7	38.80
5 wt% Y_2O_3-10 wt% AlN-Al_2O_3 [25]	cold isostatic pressing	475.61 ± 21.56	34.21 ± 0.34
20 vol% AlN-80 vol% Al_2O_3 [38]	vacuum hot pressing	432.65 ± 21.67	-
5 wt% Y_2O_3-15 wt% AlN-Al_2O_3	DLP	572.73 ± 59.40	31.72 ± 0.45

Complex-shaped Al_2O_3-AlN composites ceramic components were fabricated via DLP with the optimized AlN content and sintering temperature. The green bodies of ceramic radiators with different shapes and lattice structures are presented in Figure 9a,c. The sintering bodies are shown in Figure 9b,d. The green and sintering bodies show great surface quality and no significant geometric deformation. The shrinkage of the samples after sintering in the x, y, and z directions reached 20.25%, 20.34%, and 21.38%, respectively. Complex-shaped and high-precision ceramics components, with 15 wt% AlN addition, are able to be fabricated by DLP and achieve high bending strength and high thermal conductivity.

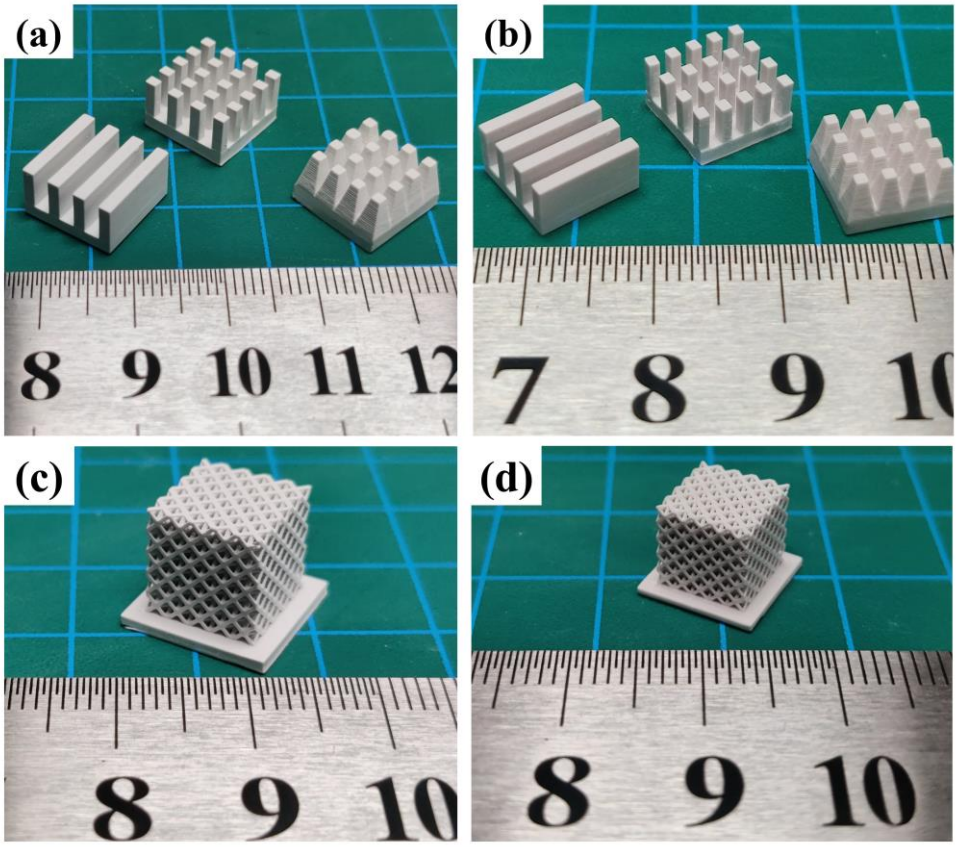


Figure 9. Al_2O_3-AlN ceramic components with complex shapes fabricated by DLP: (**a**) Green bodies of heat dissipations before sintering; (**b**) Sintering body of (**a**); (**c**) Green body of lattice structure; (**d**) Sintering body of (**c**).

4. Conclusions

In this study, the effect of AlN content (0–20 wt%) on the rheological behavior, stability, and curing behavior of Al_2O_3-AlN ceramic suspensions were investigated. The viscosity of suspensions with AlN additions decreased due to the lower friction between the particles. However, the addition of AlN increased the absorbance of ceramic powders, resulting in the decline of the curing ability of Al_2O_3-AlN suspensions. As the content of AlN powders increased from 0 to 20 wt%, S_d, S_w and D_b decreased from 50.06 to 25.07 μm, 101.39 to 56.62 μm, and 42.23 to 19.36 μm, respectively, which is beneficial to control print precision. Moreover, relative density, thermal conductivity and bending strength of Al_2O_3-AlN composites fabricated by DLP were discussed. The addition of AlN is beneficial for improving relative density, while the densification of Al_2O_3-AlN ceramics will be affected when the content of AlN reaches 20 wt%. The increase of AlN content resulted in the improvement of the thermal conductivity of Al_2O_3-AlN ceramics at 1650 °C. The bending strength of Al_2O_3-AlN ceramics was enhanced with the content of AlN increasing from 0 to 15 wt%, which is due to grains refining and residual stress. Thus, 15 wt% is the optimum content of AlN by comprehensively considering the printability of suspensions and properties of Al_2O_3-AlN composite ceramics. The 5 wt% Y_2O_3-15 wt% AlN-Al_2O_3 fabricated by DLP got the best comprehensive properties in terms of the bending strength of 572.73 ± 59.40 MPa and the thermal conductivity of 31.72 ± 0.45 W/(m·K) at 1650 °C. With optimized AlN content (15 wt%) and sintering temperature (1650 °C), complex-shaped ceramic components were successfully fabricated by DLP. Ceramic components fabricated by this approach achieved excellent surface quality and structural integrity (no significant geometric deformation). This may provide an opportunity to broaden the application of Al_2O_3-AlN composite ceramics in heat dissipation components.

Author Contributions: Conceptualization, S.H. and Y.L.; Methodology, S.H. and Y.L.; Software, S.H.; Investigation, S.H., Y.L. and S.W.; Formal analysis, S.H., X.Z. and S.W.; Resources, S.W.; Data Curation, S.H., Y.L. and X.Z.; Writing—review and editing, S.H. and X.Z.; Supervision, X.Z.; Project administration, S.W. and X.Z.; Funding acquisition, S.W. All authors have read and agreed to the published version of the manuscript.

Funding: This work was funded by the Local Innovative Research Team Project of the Guangdong Pearl River Talents Program (Grant No.2017BT01C169), Key-Area Research and Development Program of Guangdong Province (Grant No.2020B090923002), Foshan Science and Technology Innovation Team project (Grant No. FS0AA-KJ919-4402-0023), and Xijiang Innovation Team Introduction Program of Zhaoqing.

Data Availability Statement: The data presented in this study are available on request from the corresponding authors. The data are not publicly available due to the fact that the research is still in progress.

Conflicts of Interest: The authors declare no conflict of interest.

References

1. Nieto, M.I.; Martínez, R.; Mazerolles, L.; Baudín, C. Improvement in the thermal shock resistance of alumina through the addition of submicron-sized aluminium nitride particles. *J. Eur. Ceram. Soc.* **2004**, *24*, 2293–2301. [CrossRef]
2. Ge, R.; Zhang, Y.; Liu, Y.; Fang, J.; Luan, W.; Wu, G. Effect of Gd_2O_3 addition on mechanical, thermal and shielding properties of Al_2O_3 ceramics. *J. Mater. Sci.-Mater. Electron.* **2017**, *28*, 5898–5905. [CrossRef]
3. Lin, K.; Nie, G.; Sheng, P.; Zhao, S.; Wu, S. Effects of doping Al-metal powder on thermal, mechanical and dielectric properties of AlN ceramics. *Ceram. Int.* **2022**, *48*, 36210–36217. [CrossRef]
4. Lin, L.; Wu, H.; Ni, P.; Chen, Y.; Huang, Z.; Li, Y.; Lin, K.; Sheng, P.; Wu, S. Additive manufacturing of complex-shaped and high-performance aluminum nitride-based components for thermal management. *Addit. Manuf.* **2022**, *52*, 102671. [CrossRef]
5. Van Roekeghem, A.; Vermeersch, B.; Carrete, J.; Mingo, N. Thermal Resistance of GaN/AlN Graded Interfaces. *Phys. Rev. Appl.* **2019**, *11*, 034036. [CrossRef]
6. Huang, S.; Gao, F.; Li, Q.; Cheng, X. AlON phase formation in hot-pressing sintering Al_2O_3/AlN composites and their oxidation behavior. *J. Alloys Compd.* **2016**, *685*, 309–315. [CrossRef]
7. Kim, M.K.; Lee, B.; Koo, M.Y.; Ryu, H.J.; Hong, S.H. Fabrication of Al_2O_3/AlN micro-composites designed for tailored physical properties. *Mater. Des.* **2015**, *86*, 1–5. [CrossRef]

8. Scheithauer, U.; Schwarzer, E.; Moritz, T.; Michaelis, A. Additive Manufacturing of Ceramic Heat Exchanger: Opportunities and Limits of the Lithography-Based Ceramic Manufacturing (LCM). *J. Mater. Eng. Perform.* **2017**, *27*, 14–20. [CrossRef]
9. Sun, L.; Dong, P.; Zeng, Y.; Chen, J. Fabrication of hollow lattice alumina ceramic with good mechanical properties by Digital Light Processing 3D printing technology. *Ceram. Int.* **2021**, *47*, 26519–26527. [CrossRef]
10. Ruiz-Morales, J.C.; Tarancón, A.; Canales-Vázquez, J.; Méndez-Ramos, J.; Hernández-Afonso, L.; Acosta-Mora, P.; Marín Rueda, J.R.; Fernández-González, R. Three dimensional printing of components and functional devices for energy and environmental applications. *Energy Environ. Sci.* **2017**, *10*, 846–859. [CrossRef]
11. Varghese, G.; Moral, M.; Castro-García, M.; López-López, J.J.; Marín-Rueda, J.R.; Yagüe-Alcaraz, V.; Hernández-Afonso, L.; Ruiz-Morales, J.C.; Canales-Vázquez, J. Fabrication and characterisation of ceramics via low-cost DLP 3D printing. *Boletín Soc. Española Cerámica Vidr.* **2018**, *57*, 9–18. [CrossRef]
12. Li, H.; Liu, Y.; Liu, Y.; Hu, K.; Lu, Z.; Liang, J. Influence of Sintering Temperature on Microstructure and Mechanical Properties of Al_2O_3 Ceramic via 3D Stereolithography. *Acta Metall. Sin.* **2019**, *33*, 204–214. [CrossRef]
13. Zakeri, S.; Vippola, M.; Levänen, E. A comprehensive review of the photopolymerization of ceramic resins used in stereolithography. *Addit. Manuf.* **2020**, *35*, 101177. [CrossRef]
14. Zhang, K.; Xie, C.; Wang, G.; He, R.; Ding, G.; Wang, M.; Dai, D.; Fang, D. High solid loading, low viscosity photosensitive Al_2O_3 slurry for stereolithography based additive manufacturing. *Ceram. Int.* **2019**, *45*, 203–208. [CrossRef]
15. de Camargo, I.L.; Morais, M.M.; Fortulan, C.A.; Branciforti, M.C. A review on the rheological behavior and formulations of ceramic suspensions for vat photopolymerization. *Ceram. Int.* **2021**, *47*, 11906–11921. [CrossRef]
16. Wu, X.; Xu, C.; Zhang, Z. Preparation and optimization of Si_3N_4 ceramic slurry for low-cost LCD mask stereolithography. *Ceram. Int.* **2021**, *47*, 9400–9408. [CrossRef]
17. Lin, L.; Wu, H.; Huang, Z.; Wu, S. Effect of monomers with different functionalities on stability, rheology, and curing behavior of ceramic suspensions. *Mater. Chem. Phys.* **2022**, *275*, 125243. [CrossRef]
18. Zou, W.; Yang, P.; Lin, L.; Li, Y.; Wu, S. Improving cure performance of Si_3N_4 suspension with a high refractive index resin for stereolithography-based additive manufacturing. *Ceram. Int.* **2022**, *48*, 12569–12577. [CrossRef]
19. Boey, F.; Cao, L.; Khor, K.A.; Tok, A. Phase reaction and sintering behavior of a Al_2O_3–20 wt%AlN–5 wt%Y_2O_3 system. *Acta Mater.* **2001**, *49*, 3117–3127. [CrossRef]
20. Kim, Y.W.; Park, H.C.; Lee, Y.B.; Oh, K.D.; Stevens, R. Reaction sintering and microstructural development in the system Al_2O_3–AlN. *J. Eur. Ceram. Soc.* **2001**, *21*, 2383–2391. [CrossRef]
21. Hu, J.; Huang, Q.; Peng, H.; Tian, X.; Chen, Z.; Peng, Y. Effect of AlN content on the properties and microstructure of pressureless-sintered Al_2O_3-AlN composites. *J. Ceram. Process. Res.* **2018**, *19*, 224–230.
22. Zhou, M.; Liu, W.; Wu, H.; Song, X.; Chen, Y.; Cheng, L.; He, F.; Chen, S.; Wu, S. Preparation of a defect-free alumina cutting tool via additive manufacturing based on stereolithography–Optimization of the drying and debinding processes. *Ceram. Int.* **2016**, *42*, 11598–11602. [CrossRef]
23. Li, K.; Zhao, Z. The effect of the surfactants on the formulation of UV-curable SLA alumina suspension. *Ceram. Int.* **2017**, *43*, 4761–4767. [CrossRef]
24. Liu, W.; Wu, H.; Tian, Z.; Li, Y.; Zhao, Z.; Huang, M.; Deng, X.; Xie, Z.; Wu, S. 3D printing of dense structural ceramic microcomponents with low cost: Tailoring the sintering kinetics and the microstructure evolution. *J. Am. Ceram. Soc.* **2019**, *102*, 2257–2262. [CrossRef]
25. Nie, G.; Li, Y.; Sheng, P.; Tian, Z.; Liu, W.; Wu, H.; Bao, Y.; Wu, S. Fabrication of Al_2O_3/AlN composite ceramics with enhanced performance via a heterogeneous precipitation coating process. *Ceram. Int.* **2020**, *46*, 21156–21165. [CrossRef]
26. Liu, C.; Guo, W.-M.; Sun, S.-K.; Zou, J.; Wu, S.-H.; Lin, H.-T. Texture, microstructures, and mechanical properties of AlN-based ceramics with Si_3N_4-Y_2O_3 additives. *J. Am. Ceram. Soc.* **2017**, *100*, 3380–3384. [CrossRef]
27. Leitner, J.; Voňka, P.; Sedmidubský, D.; Svoboda, P. Application of Neumann–Kopp rule for the estimation of heat capacity of mixed oxides. *Thermochim. Acta* **2010**, *497*, 7–13. [CrossRef]
28. Eric, S.; Thierry, C.; Philippe, B.; Marie-Francoise, D. Densification and thermal conductivity of low-sintering-temperature AlN materials. *J. Eur. Ceram. Soc.* **1990**, *6*, 23–29.
29. Xu, X.; Zhou, S.; Wu, J.; Liu, S.; Ma, S.; Cheng, T. Study of alumina ceramic parts fabricated via DLP stereolithography using powders with different sizes and morphologies. *Int. J. Appl. Ceram. Technol.* **2022**. [CrossRef]
30. Gentry, S.P.; Halloran, J.W. Depth and width of cured lines in photopolymerizable ceramic suspensions. *J. Eur. Ceram. Soc.* **2013**, *33*, 1981–1988. [CrossRef]
31. Huang, S.; Li, Y.; Yang, P.; Sheng, P.; Ou, J.; Ning, T.; Wu, S. Cure behaviour and mechanical properties of Si_3N_4 ceramics with bimodal particle size distribution prepared using digital light processing. *Ceram. Int.* **2022**. [CrossRef]
32. Kim, Y.W.; Oh, Y.W.; Yoon, S.Y.; Stevens, R.; Park, H.C. Thermal diffusivity of reaction-sintered AlON/Al_2O_3 particulate composites. *Ceram. Int.* **2008**, *34*, 1849–1855. [CrossRef]
33. Lee, H.M.; Bharathi, K.; Kim, D.K. Processing and Characterization of Aluminum Nitride Ceramics for High Thermal Conductivity. *Adv. Eng. Mater.* **2014**, *16*, 655–669. [CrossRef]
34. Shi, X.L.; Xu, F.M.; Zhang, Z.J.; Dong, Y.L.; Tan, Y.; Wang, L.; Yang, J.M. Mechanical properties of hot-pressed Al_2O_3/SiC composites. *Mater. Sci. Eng. A* **2010**, *527*, 4646–4649. [CrossRef]

35. Hoshide, T.; Hiramatsu, H. Characterization of integrated data on inherent flaws in engineering ceramics. *Mater. Sci. Res. Int.* **1999**, *5*, 285–290. [CrossRef]
36. Wang, A.; Hu, P.; Zhao, X.; Wang, Z.; Zhang, C.; Wang, Y. Modelling and experimental investigation of pore-like flaw-strength response in structural ceramics. *Ceram. Int.* **2020**, *46*, 14431–14438. [CrossRef]
37. Luo, J.; Stevens, R. The Role of Residual Stress on the Mechanical Properties of Al_2O_3 -5vol% SiC Nano-Composites. *J. Eur. Ceram. Soc.* **1997**, *17*, 1565–1572. [CrossRef]
38. Li, Q.; Wu, C.; Wang, Z. Mechanical properties and microstructures of Nano-Al_2O_3 particles reinforced Al_2O_3/AlN composite. *J. Alloys Compd.* **2015**, *636*, 20–23. [CrossRef]

Disclaimer/Publisher's Note: The statements, opinions and data contained in all publications are solely those of the individual author(s) and contributor(s) and not of MDPI and/or the editor(s). MDPI and/or the editor(s) disclaim responsibility for any injury to people or property resulting from any ideas, methods, instructions or products referred to in the content.